



# Practical design of the QZS isolator with one pair of oblique bars by considering pre-compression and low-dynamic stiffness

Feng Zhao · Shuqian Cao · Quantian Luo · Liqing Li · Jinchen Ji

Received: 24 November 2021 / Accepted: 13 March 2022 / Published online: 29 March 2022  
© The Author(s), under exclusive licence to Springer Nature B.V. 2022

**Abstract** Various quasi-zero stiffness (QZS) vibration isolators have been developed by using the structures of oblique springs and bars. Towards a practical design, this paper further theoretically and experimentally studies the static and dynamic force of the QZS isolator with one pair of oblique bars by considering pre-compression of horizontal springs and producing an extremely low-dynamic stiffness. By designing the new parameter configuration, two simple formulations are derived on the basis of two QZS conditions to design an improved QZS isolator with a constant low-dynamic stiffness in a wide region around the static equilibrium position. A detailed

comparison between the proposed and the existing isolators is made to show the significant improvement on isolation performance. On the basis of the derived formulations, a prototype is fabricated and tested to verify the theoretical formulations and constant low-dynamic stiffness. The experimental results show that the designed QZS isolator can achieve a much wider QZS region to isolate vibration in a larger frequency band and demonstrate a lower displacement transmissibility for the external excitation.

**Keywords** Quasi-zero stiffness · QZS isolator · Oblique bars · Low-dynamic stiffness · Vibration isolation

---

F. Zhao · S. Cao (✉) · L. Li  
Department of Mechanics, Tianjin University,  
Tianjin 300354, China  
e-mail: sqcao@tju.edu.cn

F. Zhao · S. Cao · L. Li  
Tianjin Key Laboratory of Nonlinear Dynamics and  
Control, Tianjin 300354, China

F. Zhao  
Henan Key Laboratory of Intelligent Manufacturing of  
Mechanical Equipment, College of Mechanical and  
Electrical Engineering, Zhengzhou University of Light  
Industry, Zhengzhou 450002, China

Q. Luo · J. Ji (✉)  
School of Mechanical and Mechatronic Engineering,  
University of Technology Sydney, 15 Broadway, Ultimo,  
NSW 2007, Australia  
e-mail: jin.ji@uts.edu.au

## 1 Introduction

Quasi-zero stiffness (QZS) isolators with high-static and low-dynamic stiffness are capable of supporting considerable mass load and increasing frequency band of vibration isolation and thus can solve the conflicting issue of low frequency of vibration isolation with large static displacements in using linear isolators [1–4]. The QZS isolators can be constructed using negative stiffness in parallel with positive stiffness. The positive stiffness is easily acquired using coil springs, while the negative stiffness can be achieved using oblique springs [5–8], oblique bars [9–14], cam-rollers

[15–17], magnetic springs, or bionic structures [18–23].

The majority of the existing QZS isolators have low-dynamic stiffness with weak nonlinearity [24]. For example, the classical QZS isolator with one pair of oblique springs was designed using the pre-compression and nonlinearity of the oblique springs to widen the QZS range around the static equilibrium position [5, 6, 25]. To further increase the QZS range and reduce nonlinearity, multiple pairs of oblique springs and other configurations based on one pair of oblique springs were developed [7, 8, 11, 26–28]. However, the weakly nonlinear stiffness generated often makes a transmissibility curve bend to the right under large displacement excitation, resulting in narrowing the frequency band in vibration isolation.

Another classical QZS isolator is the structure formed using oblique bars without pre-compression of horizontal springs [9, 10], which has essentially nonlinear stiffness. Subsequently, this type of QZS isolator has been studied in [3, 12, 29–37]. Theoretically, the QZS isolator with oblique bars is similar to that based on one pair of oblique springs. They have a limited QZS region around the static equilibrium position, although different negative stiffness mechanisms are constructed by using springs or bars. Bio-inspired vibration isolators were also constructed using bars and springs in order to enlarge the QZS region around the equilibrium position [21, 38–40]. Although a wide QZS range can be obtained, the weakly nonlinear stiffness around the equilibrium position remains and degrades the performance of vibration isolation under large amplitude of excitations [29, 30]. For practical applications, the QZS isolators should have a wide QZS region with a very low-dynamic stiffness and be able to isolate large amplitude of vibrations. Due to their simple configurations, the above-mentioned two classical QZS isolators could be adopted in practical engineering applications. However, it is not clear which classical QZS isolator would have a better performance, because these two classical isolators have not been quantitatively compared by using the same dimensionless parameters of equivalent physical meanings. Therefore, it is necessary to further investigate the isolation performance of these two types of QZS isolators from the perspective of practical design.

To avoid the performance degradation of vibration isolation induced by weakly nonlinear stiffness under

large amplitude of excitations, the QZS isolator with very low-dynamic stiffness (constant quasi-zero dynamic stiffness, or a constant dynamic force) around the static equilibrium position is able to achieve better performance of vibration isolation. There are many structures that can achieve constant-force mechanisms such as cam-rollers [15, 41, 42], and oblique bars [43, 44]. The QZS isolator with one pair of oblique bars could not exhibit a constant force unless the length of the oblique bar tends to zero [9, 10] (where pre-compression of the horizontal springs is not considered), which is meaningless for practical applications. The pre-compression of horizontal springs in this type of QZS isolator plays a key role in achieving the constant force feature, and the corresponding constant low-dynamic stiffness can significantly widen the QZS range around the static equilibrium position and hence enlarge the frequency band of isolate vibration. It should be mentioned that a large region of zero dynamic-stiffness could not be used for vibration isolation because of the potential unstable nature of vibration. A low-dynamic stiffness would be desirable for vibration isolation, especially in low-frequency range.

In this paper, the practical design of the QZS isolator with one pair of oblique bars is theoretically and experimentally studied by taking into account pre-compression of the horizontal springs and imposing the zero condition of the second derivative of stiffness. The QZS isolator can realize very low-dynamic stiffness (small constant stiffness) in a wide range of quasi-zero stiffness near the static equilibrium position. Here, the static equilibrium position is the initial loaded position when the two oblique bars are in horizontal directions. The novelties and main contributions are:

- (1) The design parameters of the improved isolator with one pair of oblique bars have the same physical meaning as the isolator with one pair of oblique springs. Thus, these two classical QZS isolators have the same non-dimensional parameters and can be quantitatively compared for the performance of vibration isolation. Results show that the designed isolator can easily realize constant quasi-zero stiffness in a wide region around the equilibrium position, while the isolator with one pair of oblique springs only has a narrow QZS range.
- (2) The pre-compressions of the horizontal springs are considered in the type of QZS isolator with

one pair of oblique bars to significantly improve isolation performance of the corresponding isolator in [9, 10]. Utilization of pre-compressed horizontal springs can produce a large range of constant low-dynamic stiffness which is beneficial for vibration isolation.

- (3) The second derivative of stiffness is set to be zero in determining the theoretical values of the system parameters for the designed QZS isolator, and then, two simple formulations are derived on the basis of two QZS conditions to design the QZS isolator. This condition provides a boundary/guideline for designing the system parameters. There is no need to meet this ideal condition in practical design. In fact, it is very difficult to satisfy this theoretical criterion by using off-the-shelf mechanical components. As long as the physical parameters are selected in a small neighbourhood of this theoretical boundary, the QZS isolator can achieve superior performance.
- (4) On the basis of the derived formulations, a prototype is fabricated and tested to verify the theoretical formulations and show superior isolation performance of the designed QZS isolator with one pair of oblique bars. The parameters are selected from a small neighbourhood of the theoretical guideline, and the springs are not specifically designed/manufactured but are available off the shelf.
- (5) The designed QZS isolator in this paper can easily realize constant quasi-zero stiffness, which means that a very low-dynamic stiffness is achieved in a wide region around the equilibrium position. However, the existing isolator with one pair of oblique bars and the classic isolator with one pair of oblique springs cannot achieve the constant quasi-zero stiffness around the equilibrium position.

## 2 Static analysis

### 2.1 New structure configuration for the improved QZS isolator

Figure 1a and b shows the improved QZS isolator with one pair of oblique bars and the previous design in [9, 10]. Figure 1c and d illustrates non-dimensional

force and stiffness of the proposed and previous isolators, respectively, clearly indicating the significant enhancement on QZS features. The advantages of the improved design are twofold:

- (a) By using the pre-compression of the horizontal springs, the improved design shown in Fig. 1a could realize a constant quasi-zero stiffness (i.e. a constant low-dynamic stiffness in a large range), or zero dynamic stiffness under ideal conditions. On the contrary, the previous design only demonstrates a small range of quasi-zero stiffness.
- (b) In the improved design, the second derivative of stiffness is set to be zero, and thus, two simple formulations of obtaining low-dynamic stiffness (or zero dynamic stiffness) are derived. Then, a constant quasi-zero stiffness can be easily achieved for practical design and realized by using mechanical structures.

In the improved design shown in Fig. 1a (the system is at the initial unloaded position), two oblique bars intersect at a point  $O$  and the negative stiffness in the vertical direction will be generated when force  $f$  is applied on the top of the oblique bars and the horizontal spring will generate the restoring force on the bottom of the oblique bar. The horizontal spring restoring force is generated by an elastic element with linear stiffness coefficient  $k_1$  and pre-compression  $\delta$ . The elastic element can be either compression or extension springs. The negative stiffness is parallel with the linear positive stiffness  $k_2$  to generate QZS. At the initial unloaded point  $O$ , the vertical spring (linear spring) is in its free position. The displacement from the initial position is defined as  $x$ , and the displacement from the static equilibrium position is denoted by  $y$ . The distance from the initial position to the static equilibrium position is  $h$  as shown in Fig. 1a. The horizontal distance of the oblique bar at the initial position is referred to as  $a$ . When a suitable mass is loaded on point  $O$ , the isolator will be at the static equilibrium position where the oblique bars are in horizontal direction.

### 2.2 Force analysis

For the isolator shown in Fig. 1a, the applied force  $f$  and displacement  $x$  from the initial position can be derived by using the principle of virtual work:

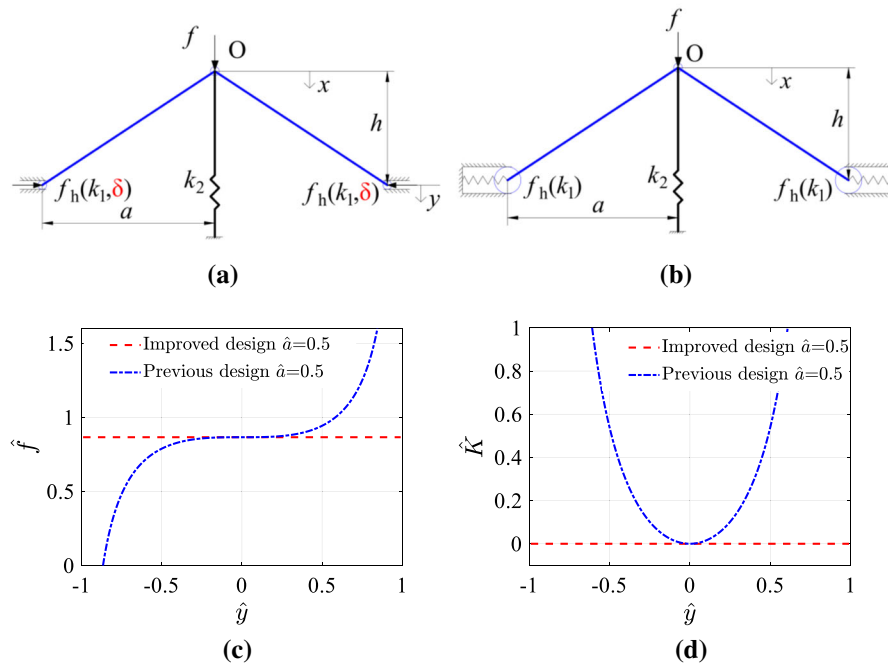


**Fig. 1** The QZS isolator with one pair of oblique bars **a** the improved design, **b** the previous design [9, 10], **c** force–displacement curves of the previous and improved designs, **d** stiffness–displacement curves of the previous and improved designs

$$(f + f_2 + 2f_{1x})\Delta x = 0 \tag{1}$$

in which,

$$\begin{cases} f_2 = -k_2x \\ f_{1x} = -f_1 \frac{h-x}{\sqrt{a^2+h^2}} \end{cases} \tag{2}$$

where  $f_2$  is the vertical force generated from the vertical spring having the stiffness of  $k_2$ .  $f_1$  denotes the axial force provided by the oblique bar, and  $f_{1x}$  is the vertical force component from the oblique bars. The horizontal force  $f_h$ , generated by the pre-compression of the horizontal springs, can be derived as:

$$\begin{cases} f_1 = f_h \frac{\sqrt{a^2+h^2}}{\sqrt{\sqrt{a^2+h^2} - (h-x)^2}} \\ f_h = k_1 \left( \sqrt{\sqrt{a^2+h^2} - (h-x)^2} - a + \delta \right) \end{cases} \tag{3}$$

The horizontal force  $f_h$  of the previous design [9, 10] without pre-compression is given by:

$$f_h = k_1 \left( \sqrt{\sqrt{a^2+h^2} - (h-x)^2} - a \right) \tag{4}$$

By combining Eqs. (1)–(3), force  $f$  of the improved design can be derived as:

$$f = k_2x + 2k_1 \left( \frac{\sqrt{\sqrt{a^2+h^2} - (h-x)^2} - a + \delta}{h-x} \right) \frac{1}{\sqrt{\sqrt{a^2+h^2} - (h-x)^2}} \tag{5}$$

For the understanding of the force around the static equilibrium position, Eq. (5) can be expressed as:

$$f = k_2h + \left( k_2y - 2k_1 \left( \sqrt{\sqrt{a^2+h^2} - y^2} - a + \delta \right) \frac{y}{\sqrt{\sqrt{a^2+h^2} - y^2}} \right) \tag{6}$$

where  $y$  is the displacement of the isolator from the static equilibrium position, which satisfies the relationship of  $y = x - h$ . Equation (6) has two components. The first term is equivalent to the constant mass load of  $mg$ . The second term is the dynamic force generated around the static equilibrium position.

If the pre-compression  $\delta$  is zero, Eq. (5) or (6) degenerates to the force formulation of the previous design. Equation (5) can be further expressed in a non-dimensional form by dividing  $k_2\sqrt{a^2 + h^2}$ :

$$\hat{f} = \hat{x} + 2\alpha p_1 \frac{\sqrt{1 - p_1^2} - \hat{a} + \hat{\delta}}{\sqrt{1 - p_1^2}} \tag{7}$$

Due to  $\hat{y} = \hat{x} - \sqrt{1 - \hat{a}^2}$  and  $\frac{h}{\sqrt{a^2+h^2}} = \sqrt{1 - \hat{a}^2}$ , Eq. (7) can be rewritten in terms of coordinate  $\hat{y}$  as:

$$\hat{f} = \sqrt{1 - \hat{a}^2} + \left( 1 - 2\alpha \frac{\sqrt{1 - \hat{y}^2} - \hat{a} + \hat{\delta}}{\sqrt{1 - \hat{y}^2}} \right) \hat{y} \tag{8}$$

Equation (8) can also be derived by dividing  $k_2\sqrt{a^2 + h^2}$  on both sides of Eq. (6). The first term in Eq. (8) is the constant mass load. The second term is the dynamic force. Thus, Eqs. (7) and (8) are same in essence, although different coordinates are used in the equations. In which,  $\hat{f} = \frac{f}{k_2\sqrt{a^2+h^2}}$ ,  $\hat{x} = \frac{x}{\sqrt{a^2+h^2}}$ ,  $\hat{y} = \frac{y}{\sqrt{a^2+h^2}}$ ,  $\alpha = \frac{k_1}{k_2}$ ,  $\hat{a} = \frac{a}{\sqrt{a^2+h^2}}$ ,  $\hat{\delta} = \frac{\delta}{\sqrt{a^2+h^2}}$ ,

$p_1 = q_1 - \hat{x}$ ,  $q_1 = \sqrt{1 - \hat{a}^2}$ .  $\hat{x}$  is the non-dimensional displacement of the isolator from the initial position;  $\alpha$  refers to the stiffness ratio between the horizontal springs and the vertical spring;  $\hat{a}$  indicates the non-dimensional length of oblique bars in the horizontal direction, and its value is in the range of (0 1);  $\hat{\delta}$  denotes the non-dimensional pre-compressed length of the horizontal spring or non-dimensional extended length of the horizontal extension spring, and its value is in the range of [0 1]. The non-dimensional stiffness  $\hat{K}$  can be derived by differentiating  $\hat{f}$  of Eq. (7) with respect to  $\hat{x}$  as:

$$\hat{K} = 1 - 2\alpha \left( 1 + (\hat{\delta} - \hat{a})(1 - p_1^2)^{-\frac{1}{2}} \right) - 2\alpha p_1^2 (\hat{\delta} - \hat{a})(1 - p_1^2)^{-\frac{3}{2}} \tag{9}$$

Equation (9) can also be expressed in terms of coordinate  $\hat{y}$  as:

$$\hat{K} = 1 - 2\alpha \left( 1 + (\hat{\delta} - \hat{a})(1 - \hat{y}^2)^{-\frac{1}{2}} \right) + \hat{y}^2 (\hat{\delta} - \hat{a})(1 - \hat{y}^2)^{-\frac{3}{2}} \tag{10}$$

Equation (10) can also be derived via differentiating  $\hat{f}$  of Eq. (8) with respect to  $\hat{y}$ . Thus, Eqs. (9) and (10) would give the same value of the dynamic stiffness, although different coordinates are involved in these equations.

If the pre-compression is zero, Eq. (9) or Eq. (10) is simplified into the stiffness formulation of the isolator in [9, 10] with only two independent parameters  $\alpha$  and  $\hat{a}$ . The non-dimensional stiffness  $\hat{K}$  in Eq. (10) for the improved design has three independent parameters of  $\hat{a}$ ,  $\hat{\delta}$  and  $\alpha$ , two of which can be eliminated by using two QZS conditions. The first QZS condition is  $\hat{K} = 0$  at the static equilibrium position by combining with Eq. (10), and the following parameter relationship can be derived as:

$$\alpha = \frac{1}{2(1 - \hat{a} + \hat{\delta})} \tag{11}$$

The second condition to realize a wider QZS range is  $\frac{d^2\hat{K}}{d\hat{x}^2} = 0$  at the static equilibrium position by combining with Eq. (10), and the second parameter condition can be derived as:

$$\hat{\delta} = \hat{a} \tag{12}$$

For the previous design shown in Fig. 1b without the pre-compression, the condition of  $\frac{d^2\hat{K}}{d\hat{x}^2} = 0$  leads to  $6\alpha\hat{a} = 0$ , which is impractical in physics, and thus, the previous design without pre-compression of the horizontal springs cannot achieve the condition of  $\frac{d^2\hat{K}}{d\hat{x}^2} = 0$ . Substituting Eq. (12) into (11) yields:

$$\alpha = 0.5 \tag{13}$$

The simple formulations in Eqs. (12) and (13) show that the optimal parameters of the improved isolator can be easily designed. The previous design in [9, 10] only utilized the QZS condition of  $\hat{K} = 0$ , and the dynamic stiffness of this type of isolator could realize QZS stiffness only in a narrow region around the static equilibrium position.

### 2.3 Parameter study on the constant quasi-zero stiffness

For the improved isolator shown in Fig. 1a, the influences of parameters on the dynamic stiffness are studied in this section. The constant quasi-zero stiffness around the static equilibrium position is an important feature for vibration isolation, which can not only decrease the resonant frequency but also widen frequency range of vibration isolation under high excitation amplitudes.

#### 2.3.1 Stiffness feature under the condition of $\widehat{K} = 0$

Parameter  $\alpha$  in Eq. (11) is derived from the first QZS condition of  $\widehat{K} = 0$  for the improved QZS isolator with one pair of oblique bars shown in Fig. 1a. Figure 2a shows the relationship of parameters  $\alpha$  and  $\widehat{a}$ . A greater value of  $\widehat{\delta}$  leads to flattening the  $\alpha - \widehat{a}$  curve.  $\alpha$  decreases with an increase of  $\widehat{\delta}$  as shown in Fig. 2b. The influence of  $\widehat{a}$  on  $\alpha$  is opposite to that of  $\widehat{\delta}$  on  $\alpha$ .

There are two independent parameters  $\widehat{\delta}$  and  $\widehat{a}$  under the QZS condition of  $\widehat{K} = 0$  at the static equilibrium position. The two independent parameters  $\widehat{\delta}$  and  $\widehat{a}$  should ensure a positive  $\alpha$  and positive dynamic stiffness around the static equilibrium position. However, not all combinations of  $\widehat{a}$  and  $\widehat{\delta}$  can obtain positive stiffness around the static equilibrium position as shown in Fig. 3. For example, a combination of  $\widehat{a} = 0.85$  and  $\widehat{\delta} = 0.9$  results in negative stiffness, and thus, it is not practical to load mass for vibration isolation.

Mathematically, the two independent parameters  $\widehat{\delta}$  and  $\widehat{a}$  under the QZS condition of  $\widehat{K} = 0$  are in the ranges of  $\widehat{\delta} \in [0, 1]$  and  $\widehat{a} \in (0, 1)$ , and the dynamic stiffness  $\widehat{K}$  near the static equilibrium position must be positive. The red line of 45-degree angle is the critical threshold for the positive stiffness as shown in Fig. 4a. When the independent parameter  $\widehat{\delta}$  is less than the independent parameter  $\widehat{a}$ , the positive stiffness around the static equilibrium position can be obtained. If  $\widehat{\delta}$  is larger than  $\widehat{a}$ , the stiffness near the static equilibrium position is negative. When  $\widehat{a} = \widehat{\delta}$ , a straight line of stiffness curve can be obtained, as shown in Fig. 4. This straight line gives zero dynamic stiffness and separates the parameters into two regions. For vibration isolation purpose, a perfect zero dynamic stiffness may induce unstable vibrations, instead a small and constant value of low-dynamic stiffness is preferred in the practical design.

A surface of parameter  $\alpha$  for the improved QZS isolator with one pair of oblique bars can be calculated by using Eq. (11), and the positive stiffness condition is shown in Fig. 5. There are many parameter combinations to generate the QZS feature around the static equilibrium position. However, the parameter combinations may lead to QZS with a third-order nonlinearity for the QZS isolator if only the first QZS condition of  $\widehat{K} = 0$  is considered.

#### 2.3.2 Stiffness feature under the condition of $\frac{d^2\widehat{K}}{dx^2} = 0$

When the parameter values of the improved design satisfy the condition of  $\frac{d^2\widehat{K}}{dx^2} = 0$ , the relationship of

**Fig. 2** Influence of parameters  $\widehat{\delta}$  and  $\widehat{a}$  on  $\alpha$  for the improved QZS isolator composed of one pair of oblique bars, **a** under the fixed values of  $\widehat{\delta}$ , **b** under the fixed values of  $\widehat{a}$

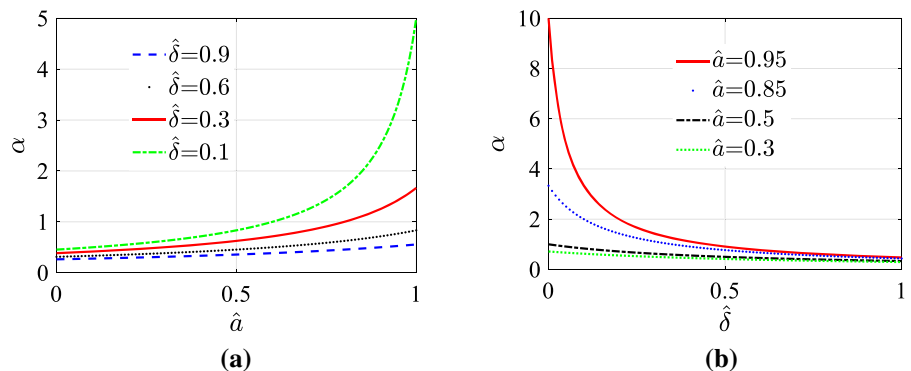


**Fig. 3** Stiffness and force curves under the first QZS condition of  $\hat{K} = 0$ , **a** stiffness–displacement curves under  $\hat{a} = 0.95$ , **b** force–displacement curves under  $\hat{a} = 0.95$ , **c** stiffness–displacement curves under  $\hat{a} = 0.85$ , **d** force–displacement curves under  $\hat{a} = 0.85$

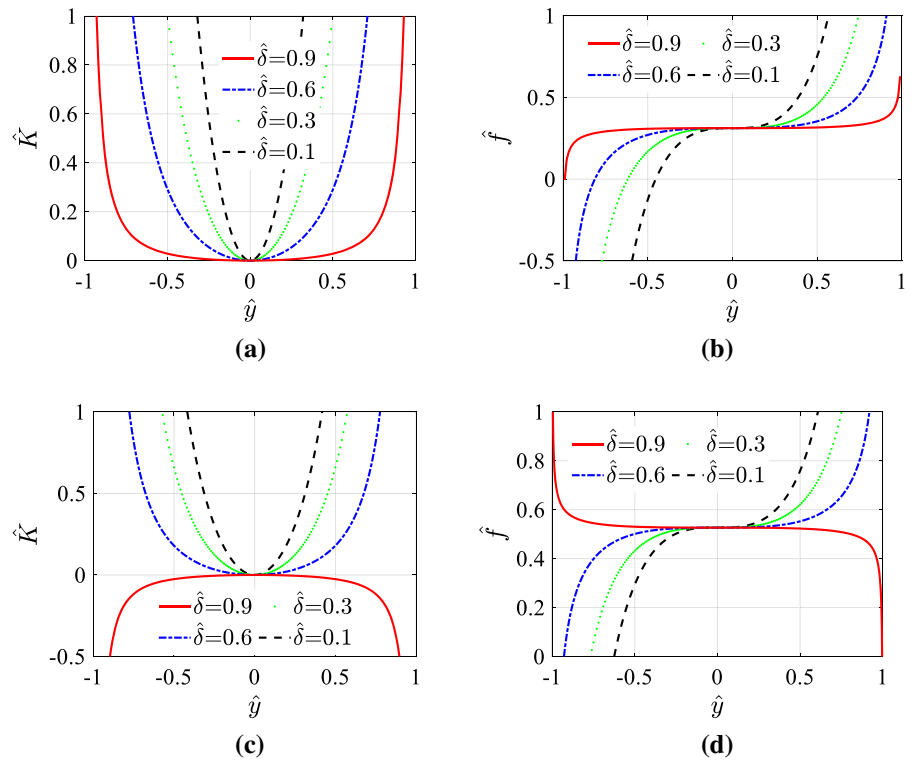
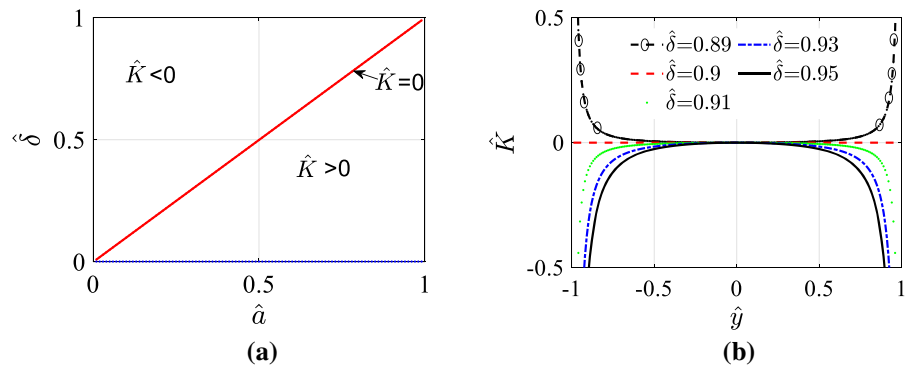


**Fig. 4** Parameter range and stiffness curves, **a** regions of independent parameters  $\hat{\delta}$  and  $\hat{a}$  for positive stiffness, **b** stiffness curves under  $\hat{a} = 0.9$  and different values of  $\hat{\delta}$



parameters  $\hat{a}$  and  $\hat{\delta}$  is  $\hat{\delta} = \hat{a}$  as given in Eq. (12). In this subsection, the condition of  $\alpha = 0.5$  as given in Eq. (13) is not imposed. A constant positive or negative stiffness will be produced. For the given values of  $\hat{a}$  and  $\hat{\delta}$ , the curves of  $\hat{K} \sim \hat{y}$  for different values of  $\alpha$  are horizontal lines with positive or negative values, and the corresponding curves of  $\hat{f} \sim \hat{y}$  are the inclined lines with positive or negative slopes as shown in Fig. 6.

For the values of  $\alpha$  ( $\alpha \neq 0.5$ ), the curves of  $\hat{K} \sim \hat{y}$  for different values of  $\hat{a} = \hat{\delta}$  are the same horizontal lines with positive or negative values, and the corresponding curves of  $\hat{f} \sim \hat{y}$  are the inclined line with positive or negative slopes, as shown in Fig. 7. Parameter  $\alpha$  does not influence the load capacity of the static equilibrium position, and parameters  $\hat{a}$  and  $\hat{\delta}$  do not affect the value of the constant dynamic stiffness. In this situation, a constant quasi-zero stiffness can be obtained in a large range for vibration isolation.

2.3.3 Stiffness feature under the conditions of  $\widehat{K} = 0$  and  $\frac{d^2\widehat{K}}{dx^2} = 0$

Equation (11) derived from  $\widehat{K} = 0$  and Eq. (12) derived from  $\frac{d^2\widehat{K}}{dx^2} = 0$  are both used to design the improved isolator. Thus,  $\alpha = 0.5$  and  $\widehat{a} = \widehat{\delta}$  are simultaneously satisfied, and then, there is only one independent parameter  $\widehat{a}$  to design the QZS isolator. In

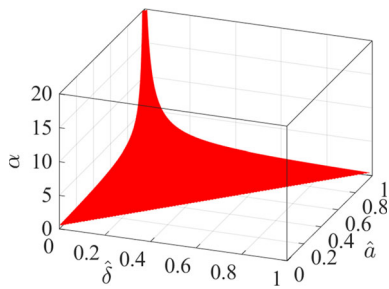
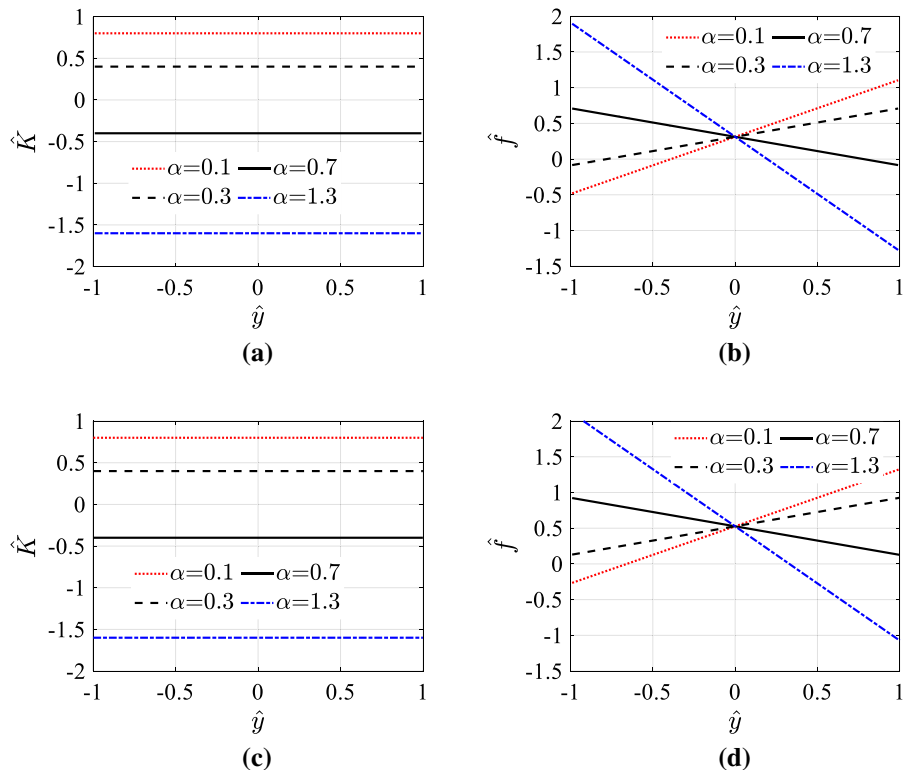


**Fig. 5** Parameter surface  $\alpha(\widehat{a}, \widehat{\delta})$  for the QZS isolator composed of one pair of oblique bars based on the conditions of  $\widehat{K} = 0$  and positive stiffness

**Fig. 6** **a** stiffness–displacement curves under  $\widehat{a} = \widehat{\delta} = 0.95$ , **b** force–displacement curves under  $\widehat{a} = \widehat{\delta} = 0.95$ , **c** stiffness–displacement curves under  $\widehat{a} = \widehat{\delta} = 0.85$ , **d** force–displacement curves under  $\widehat{a} = \widehat{\delta} = 0.85$



this case, stiffness  $\widehat{K}$  is zero in the displacement range of  $(-1 \ 1)$ , and the  $\widehat{f} \sim \widehat{y}$  curves are always horizontal lines with positive values in a range of  $(0 \ 1)$ , as shown in Figs. 8a and b, respectively. Zero dynamic stiffness cannot be used for vibration isolation; instead, constant quasi-zero stiffness shown in Fig. 7a and b having a wider QZS range is beneficial for vibration isolation. The constant quasi-zero stiffness (i.e. a very low-dynamic stiffness) can be easily realized for the QZS isolator with one pair of oblique bars when  $\widehat{a} = \widehat{\delta}$ ,  $\alpha < 0.5$ , and  $\alpha$  is close to 0.5.

In the force–displacement curves shown in Fig. 8b, the values of  $\widehat{f}$  vary with  $\widehat{a}$ . In general, a greater value of  $\widehat{a}$  leads to a smaller loading mass, which makes a higher natural frequency of the corresponding linear isolator and a wider frequency band of vibration isolation of the QZS isolator. The maximum value of  $\widehat{a}$  is 1.

In order to satisfy Eqs. (11) and (12) to realize constant quasi-zero stiffness for the improved isolator with one pair of oblique bars, the physical parameters shown in Fig. 1a should be studied to fabricate the isolator. The oblique bar has a length of  $\sqrt{a^2 + h^2}$ ,



**Fig. 7** Stiffness–displacement and force–displacement curves, **a** stiffness curves under  $\alpha = 0.4$ , **b** displacement curves under  $\alpha = 0.4$ , **c** stiffness curves under  $\alpha = 0.8$ , **d** displacement curves under  $\alpha = 0.8$

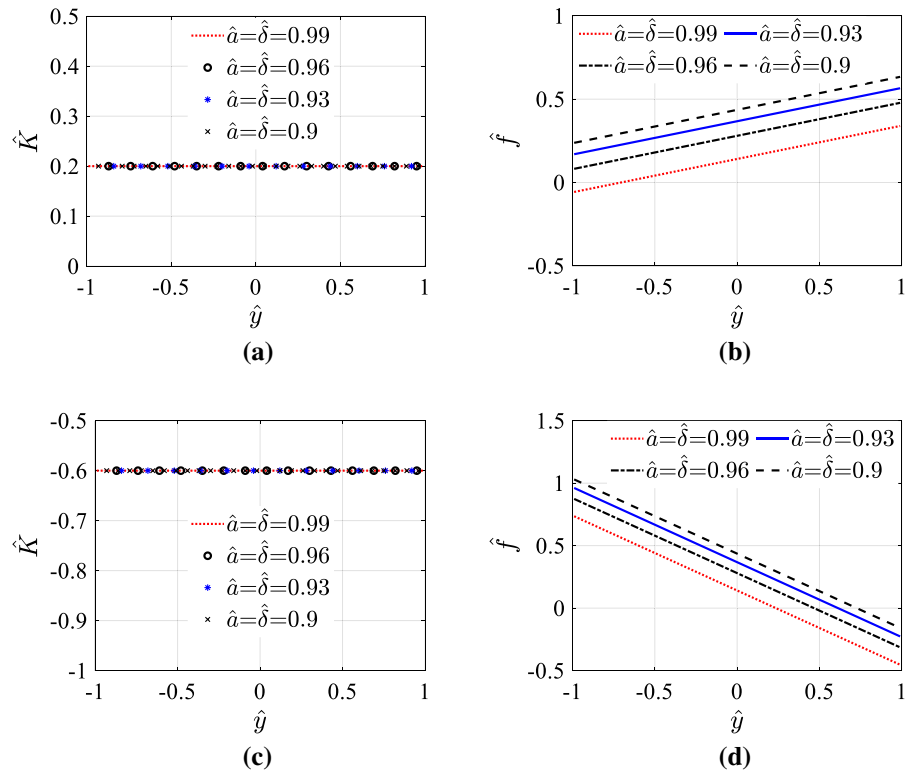
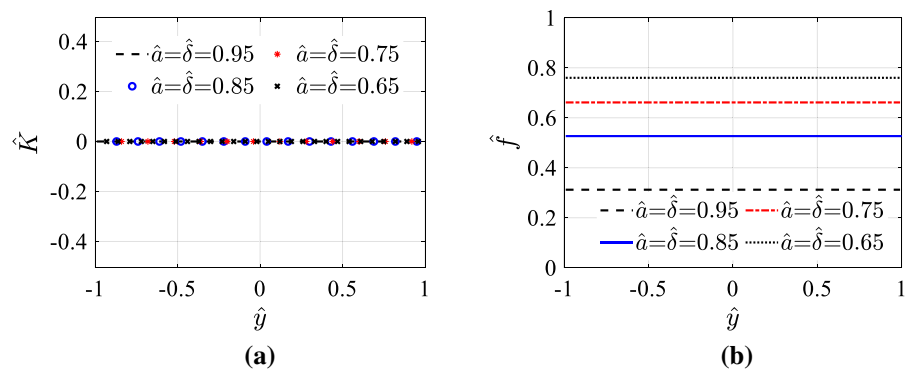


**Fig. 8** Stiffness–displacement and force–displacement curves for  $\hat{a} = \hat{\delta}$  and  $\alpha = 0.5$  **a**  $\hat{K} \sim \hat{y}$  curve for different values of  $\hat{a} = \hat{\delta}$ , **b**  $\hat{f} \sim \hat{y}$  curves for different values of  $\hat{a} = \hat{\delta}$



where  $a$  is the horizontal length of the oblique bar at the initial unloaded state. From the initial unloaded position to the static equilibrium position, the change of the horizontal length of the oblique bar is  $(\sqrt{a^2 + h^2} - a)$ , which is also the compression length of the horizontal spring on the base of  $\delta$ . If the compressible length of a metal coil spring is  $L_c$ , its pre-compressed length is  $\delta$ . For the horizontal spring, the sum of the compression length  $(\sqrt{a^2 + h^2} - a)$

and the pre-compressed length  $\delta$  should be smaller than the compressible length:

$$\sqrt{a^2 + h^2} - a + \delta < L_c \tag{14}$$

Based on the QZS conditions in Eqs. (11) and (12), Eq. (14) becomes:

$$\sqrt{a^2 + h^2} < L_c \tag{15}$$

Therefore, Eqs. (11) and (12) can be used for practical design of the QZS isolator. A low-dynamic

stiffness can be easily realized when the length of the oblique bar is smaller than the compressible length of the horizontal spring. For example, a coil spring with the free length of 90 mm has the compressible length of 50 mm, which is available for most of metal coil springs. Its pre-compression length  $\delta$  is 40 mm, and the value of  $a$  is 40 mm according to the QZS condition of Eq. (12), that is  $\hat{a} = \hat{\delta}$ . The length of the oblique bar is assumed to be 45 mm, and thus  $\hat{a} = \hat{\delta} = 0.89$ , and  $h = 20.62$  mm. Therefore, Eqs. (11) and (12) are satisfied on the basis of Eq. (15) by using widely available metal coil springs and bars. Subsequently, a constant quasi-zero stiffness can be easily realized for the QZS isolator when  $\hat{a} = \hat{\delta}$  and  $\alpha$  is slightly less than 0.5.

2.3.4 Practical design for ultra-low frequency of vibration isolation

Practical design for engineering applications is always useful. Ultra-low frequency of vibration isolation is desirable for a wide range application of QZS isolators. As shown in Fig. 9a, for a value of  $\alpha$  that is less than 0.5, the QZS isolator can achieve a very low-dynamic stiffness in a wide region. The inclined force–displacement curves can support various mass loads in a certain range as shown in Fig. 9b. Here, the supporting load is related to the value of  $\hat{f}$  at  $\hat{y} = 0$ .

The practical design for the ultra-low frequency of vibration isolation can be realized by using the QZS with a small constant value. If the loaded mass is  $m$  kg at the static equilibrium position, and the dimensional constant value of QZS is  $k_2 K_{QZS}$ . (Here,  $K_{QZS}$  is the dimensionless low-dynamic stiffness.) Thus, the frequency of vibration isolation is  $\frac{1}{\sqrt{2\pi}} \sqrt{\frac{k_2 K_{QZS}}{m}}$ . If the

desired value of ultra-low frequency of vibration isolation is  $\omega^*$ , then the vibration isolation can be realized by using

$$\frac{1}{\sqrt{2\pi}} \sqrt{\frac{k_2 K_{QZS}}{m}} \leq \omega^* \tag{16}$$

The design constant value  $K_{QZS}$  of QZS is critical to realize ultra-low frequency of vibration isolation and can be found by:

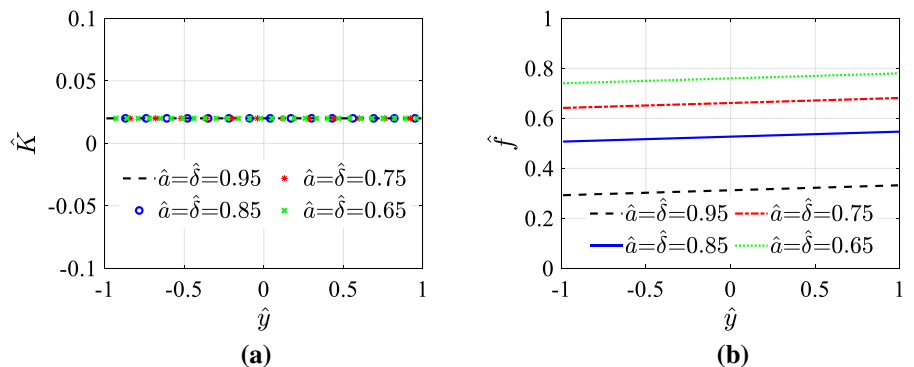
$$K_{QZS} \leq \frac{2\pi^2 m \omega^{*2}}{k_2} \text{ or } K_{QZS} \leq \frac{2\pi^2 \omega^{*2}}{\omega_0^2} \tag{17}$$

2.4 Comparison with the QZS isolator with one pair of oblique springs

Same or equivalent parameters are used for isolation performance comparison of the improved QZS isolator with one pair of oblique bars shown in Fig. 1a, and the similar QZS isolator with one pair of oblique springs [5, 25, 28] as shown in Fig. 10. For the improved QZS isolator shown in Fig. 1a, the horizontal length of oblique bar can be changed in a range of  $[a, \sqrt{a^2 + h^2}]$  in the working state. However, the horizontal length  $a$  of the QZS isolator with one pair of oblique springs does not change in the working state. From the initial unloaded position to the static equilibrium position, the length of oblique bar does not change for the improved QZS isolator, whereas the length of the oblique spring changes for the isolator with one pair of oblique springs.

By using the same parameters at the initial unloaded position and the same non-dimensional form between the two isolators shown in Figs. 1a and 10, force, stiffness and transmissibility of the two isolators

Fig. 9 Stiffness–displacement and force–displacement curves for  $\hat{a} = \hat{\delta}$  and  $\alpha = 0.49$  a  $\hat{K} \sim \hat{y}$  curve for different values of  $\hat{a} = \hat{\delta}$ , b  $\hat{f} \sim \hat{y}$  curves for different values of  $\hat{a} = \hat{\delta}$



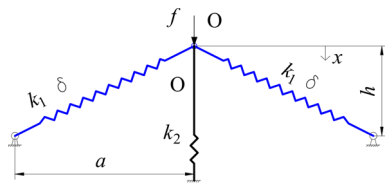


**Fig. 10** The isolator with one pair of oblique springs [6, 25]

can be quantitatively compared to show the superior performance of the improved QZS. For the isolator with one pair of oblique springs, the force and stiffness formulations under the pre-compression of oblique springs are given by

$$\begin{cases} \hat{f} = \hat{x} + 2\alpha\Gamma(\Delta - 1) \\ \hat{K} = 1 + 2\alpha\left(1 - \hat{a}\frac{\Delta}{P^2}\right) \\ \Gamma = \sqrt{1 - \hat{a}^2 - \hat{x}} \\ \Delta = \left(\frac{\hat{\delta}}{\hat{\delta} + 1}\right)/P \\ P = \sqrt{\hat{x}^2 - 2\sqrt{1 - \hat{a}^2}\hat{x} + 1} \end{cases} \quad (18)$$

The parameters  $\hat{a}$ ,  $\hat{\delta}$  and  $\alpha$  in Eqs. (18) are the same as those of the improved isolator with one pair of oblique bars. For the isolator with one pair of oblique springs, according to the QZS condition of  $\hat{K} = 0$  at the static equilibrium position, one parameter relationship is obtained as

$$\alpha = \frac{\hat{a}}{2(1 - \hat{a} + \hat{\delta})} \quad (19)$$

Under the same condition of  $\hat{K} = 0$ , Eq. (19) is different from Eq. (11) which is derived from the improved isolator shown in Fig. 1a.

The second condition of  $\frac{d^2\hat{K}}{d\hat{x}^2} = 0$  could not be imposed for the isolator with one pair of oblique springs [8] because  $\frac{d^2\hat{K}}{d\hat{x}^2} = \frac{6\alpha(1+\hat{\delta})}{a}$  is always positive. This indicates the isolator with one pair of oblique springs is unable to achieve a wider QZS range (a constant value of QZS) around the static equilibrium position. On the contrary, the improved isolator with one pair of oblique bars can exhibit a wider constant QZS range.

Based on Eqs. (7), (9) and (18), the force–displacement and stiffness–displacement curves of the two isolators shown in Figs. 1a and 10 are plotted in Fig. 11 using the parameter values in Table 1 of

Sect. 4. The force of the isolator with one pair of oblique springs in Fig. 10 to the third-order term is calculated as:

$$f_{\text{third-order}} = 0.1091 + 0.2477y + 0.7942y^3 \quad (20)$$

Equation (20) is plotted in Fig. 11a and will also be used for calculating the transmissibility. It can be seen from Fig. 11 that the improved isolator with one pair of oblique bars can realize a low-dynamic-stiffness in a wide region around the static equilibrium position and thus has a wider QZS range. Therefore, it can achieve better isolation performance as compared to the isolator with one pair of oblique springs in Fig. 10.

### 3 Dynamic analysis

#### 3.1 The equation of motion and displacement transmissibility

Generally, if a suitable magnitude of mass is placed on a QZS isolator at the initial position, the isolator will move to its static equilibrium position after the supported mass is loaded. The equation of motion of the supported mass is written as [12]

$$m\ddot{z} + c\dot{z} + f = mg \quad (21)$$

If the dynamic stiffness of the QZS isolator is kept up to the third-order nonlinear term, under the harmonic excitation of displacement, the equation of motion of the QZS isolator can be further expressed as [45]:

$$m\ddot{z} + c\dot{z} + k_L z + k_{NL} z^3 = m\omega^2 Z_e \cos(\omega t) \quad (22)$$

where  $z = z_e - y$  denotes the relative displacement;  $y$  is the absolute displacement from the static equilibrium position;  $z_e$  represents the displacement excitation;  $Z_e$  is the amplitude of  $z_e$ ;  $\omega$  is the excitation frequency of  $z_e$ ;  $c$  denotes the damping;  $k_L z$  and  $k_{NL} z^3$  are the linear and nonlinear terms of the Taylor series of dynamic force.

By dividing  $k_2\sqrt{a^2 + h^2}$ , Eq. (22) can be rewritten in non-dimensional form as:

$$\ddot{\zeta} + 2\zeta\dot{\zeta} + \mu_1\bar{z} + \mu_3\hat{z}_e^2\bar{z}^3 = \Omega^2 \cos\Omega\tau \quad (23)$$

where,  $\omega_0 = \sqrt{k_2/m}$ ,  $\Omega = \omega/\omega_0$ ,  $\tau = \omega_0 t$ ,  $\zeta = c\omega_0/2k_2$ ,  $\mu_1 = k_L/k_2$ ,  $\mu_2 = k_{NL}/k_2$ ,

**Fig. 11** Force–displacement and stiffness–displacement curves of the isolators with oblique bars and oblique springs as shown in Figs. 1a and 10, respectively

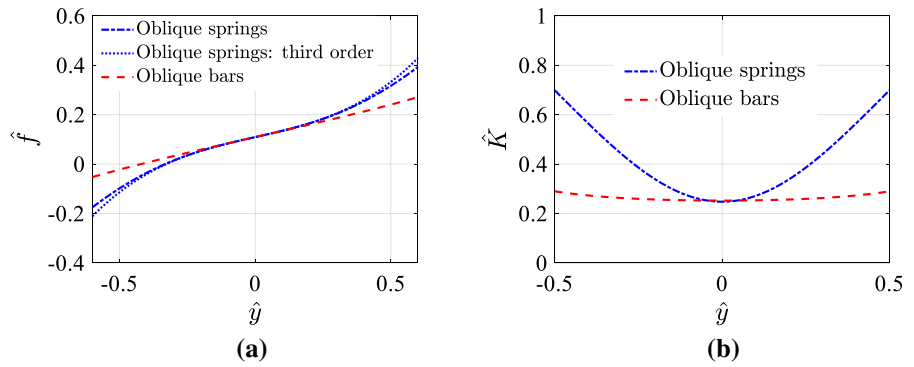


**Table 1** Parameter values of the experimental prototype of the improved isolator composed of one pair of oblique bars having a constant QZS in a wide range

$h(\text{mm})$	$a(\text{mm})$	$\delta(\text{mm})$	$k_1(\text{N/mm})$	$k_2(\text{N/mm})$
6	54.67	50	0.76	1.86

$\hat{Z}_e = Z_e / \sqrt{a^2 + h^2}$ ,  $\hat{z} = z / \sqrt{a^2 + h^2}$ ,  $\bar{z} = \hat{z} / \hat{Z}_e$ ,  $\hat{\ddot{z}} = d^2 \bar{z} / d\tau^2$ ,  $\dot{\hat{z}} = d\bar{z} / d\tau$ . Here,  $\omega_0$  is the natural frequency of the corresponding linear isolator;  $\Omega$  ( $= \omega / \omega_0$ ) is the normalized excitation frequency;  $m$  is the loaded mass; and  $\zeta$  is the damping ratio.  $\mu_1$  and  $\mu_2$  denote the non-dimensional linear and nonlinear stiffness, respectively. Assuming  $\bar{z} = Z \cos(\Omega\tau + \phi)$  and using the harmonic balance method to solve Eq. (23) yields:

$$\begin{cases} \frac{3}{4} Z_e^2 \mu_3 \hat{Z}^3 + (\mu_1 - \Omega^2) \hat{Z} = \Omega^2 \cos \phi \\ -2\zeta \Omega \dot{\hat{Z}} = \Omega^2 \sin \phi \end{cases} \quad (24)$$

where  $\hat{Z}$  is the relative displacement transmissibility, and  $\phi$  is the phase difference between the excitation and response. By squaring both sides of Eqs. (24) and then adding the two resultant equations, the following polynomial equation can be derived:

$$\left( \frac{3}{4} Z_e^2 \mu_3 \hat{Z}^3 + (\mu_1 - \Omega^2) \hat{Z} \right)^2 + (2\zeta \Omega \dot{\hat{Z}})^2 - \Omega^4 = 0 \quad (25)$$

For the proposed constant QZS isolator, the nonlinear stiffness coefficients of  $\mu_3$  are zero. For the traditional QZS isolator, a smaller value of  $\mu_3$  makes transmissibility lower. The absolute displacement transmissibility of the QZS isolator is given by [45]:

$$T_a = \sqrt{1 + 2\hat{Z} \cos \phi + \hat{Z}^2} \quad (26)$$

### 3.2 Comparison of the theoretical transmissibility

#### 3.2.1 Transmissibility comparison

*between the improved and previous designs*

Under the same mass load of the improved and previous isolators shown in Figs. 1a and b, the force and stiffness curves are given in Fig. 12. The stiffness is always zero (or a small constant value) for the improved isolator with considering the pre-compression of the horizontal springs. The QZS range of the previous isolator without considering the pre-compression of the horizontal springs is narrow.

On the basis of the theoretical parameter values of  $\hat{a} = 0.4$  for the improved and previous isolators, the performance of vibration isolation is theoretically compared by computing the displacement transmissibility. The Taylor expansion of the force formulation of the previous isolator according to Eq. (7) and  $\hat{\delta} = 0$  is

$$\hat{f} = 0.9165 + 0.3333\hat{y}^3 \quad (27)$$

By combining Eqs. (26) and (27), the displacement transmissibility of the improved and previous isolators is theoretically calculated as shown in Fig. 13. Figure 13 indicates that  $T_a < 1$  for the improved isolator. Due to the small value (nearly zero) of dynamic stiffness of the improved isolator, vibration isolation can be achieved in a full frequency band, showing much better performance than the previous QZS isolator with the weakly nonlinear stiffness.

**Fig. 12** Stiffness and force curves of the improved and previous designs under the same mass load

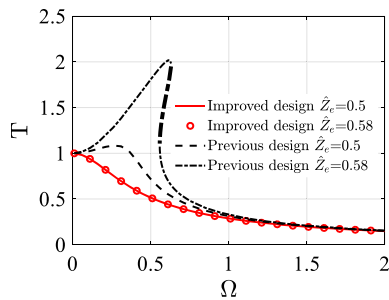
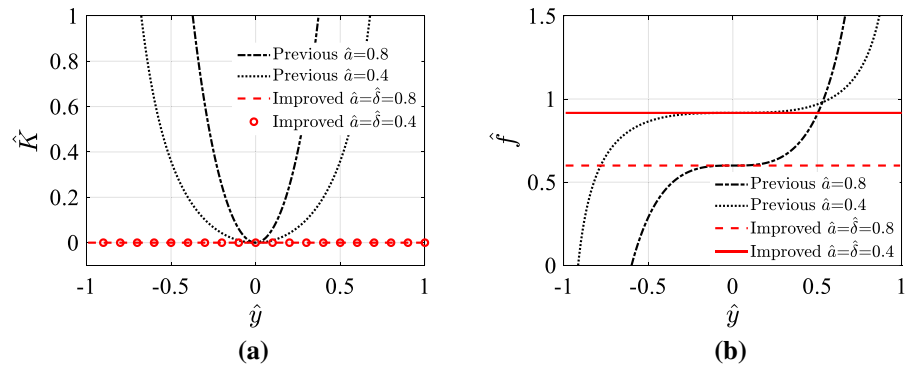


**Fig. 13** Displacement transmissibility of the improved and previous isolators

3.2.2 Theoretical transmissibility of the isolators with oblique bars and springs

On the basis of experimental parameter values in Table 1 of Sect. 4, the absolute displacement transmissibility of the isolators shown in Figs. 1a and 10 is theoretically calculated by employing Eqs. (26) and (20) and is shown in Fig. 14. For the isolator with one pair of oblique springs, the frequency band of vibration isolation is reduced under high excitation amplitude due to the weakly nonlinear stiffness.

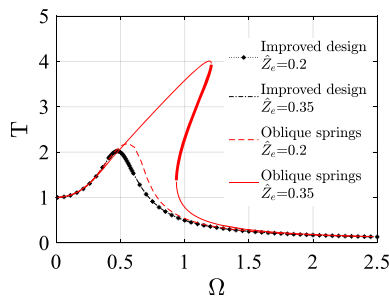


**Fig. 14** Transmissibility of the improved isolator with one pair of oblique bars and of the isolator with one pair of oblique springs for the same parameter values in Table 1

Figure 14 shows that the improved design of the isolator with one pair of oblique bars has a much wider frequency band of vibration isolation.

4 Static tests of a prototype of the improved isolator

A prototype of the improved QZS isolator with one pair of oblique bars is designed and fabricated as shown in Fig. 15. One end of the oblique bars is articulated with the mass load platform, and the other end of the oblique bars is hinged with the inner end of the horizontal movable rod. The horizontal rod can move horizontally inside the inner bearing which

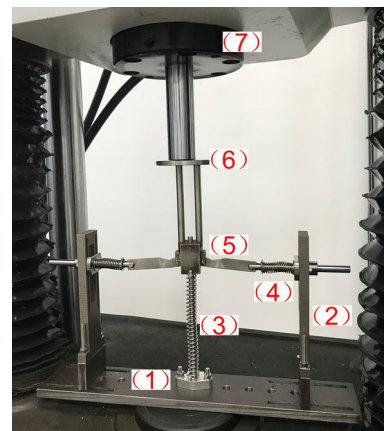


**Fig. 15** The prototype of the improved isolator tested by a universal testing machine (1) a plate to fix the QZS isolator, (2) strut frame to support the horizontal bars, (3) the vertical spring to generate positive stiffness and support the loaded mass, (4) the horizontal rods and springs to generate the horizontal force, (5) oblique bars to obtain negative stiffness in the vertical direction, (6) mass load platform, (7) universal testing machine (model WAW300, force measurement accuracy  $\pm 0.5\%$ )

provides the guideway for the horizontal springs. The horizontal springs are compressed and elongated along the horizontal movement of the rods. The oblique bars, horizontal rods and springs are assembled to generate negative stiffness. The negative stiffness is counteracted by the positive stiffness provided by the vertical spring. The vertical spring is guided by the fixed vertical rod which also provides guideway for the vertical movement of the mass load platform.

By adjusting the structural and physical parameters on the basis of Eqs. (11) and (12), the prototype can achieve QZS with a constant quasi-zero stiffness to isolate vibration with low frequency, by decreasing the horizontal length  $a$  of the oblique bar or increasing the stiffness  $k_1$  of the horizontal spring to increase the negative stiffness. Table 1 lists the design parameter values. The experimental force–displacement curves by using the universal testing machine (model WAW300) are shown in Fig. 16. As the theoretical design, the force–displacement curves are straight line with a slightly positive stiffness because the negative stiffness and perfect zero stiffness are not meaningful for vibration isolation of the loaded mass. Thus, a constant QZS is achieved from this physical model. The length of the straight line from the initial position is about 40 mm. According to Eq. (7), the theoretical force–displacement can be calculated as shown in Fig. 16 with a straight line. It is clearly shown that the experimental results are consistent and are in good agreement with the theoretical prediction.

The theoretical force–displacement curve in Fig. 16 has the non-dimensional stiffness of 0.2598, which is used to calculate the theoretical displacement

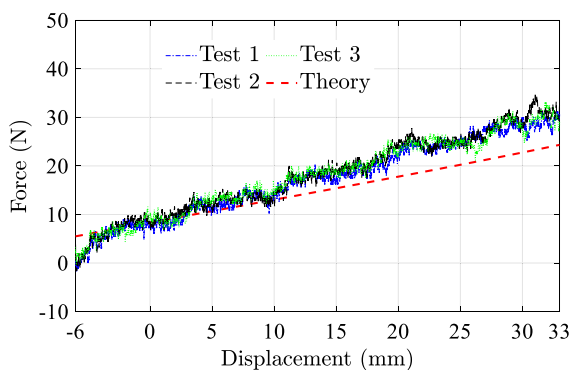


**Fig. 16** The tested and theoretical force–displacement curves for the prototype of the QZS isolator composed of one pair of oblique bars

transmissibility in the following section. The loaded mass  $m$  in the dynamic test is 1.636 kg, and the natural frequency of the corresponding linear isolator is 5.37 Hz. The QZS prototype is excited by a vibration table to verify its vibration isolation performance.

## 5 Dynamic tests to verify performance of the improved isolator

The prototype of the improved QZS isolator with one pair of oblique bars was fixed on the electric vibration table (Su Shi Testing Instrument Co Ltd) as shown in Fig. 17. A suitable mass was attached on the isolator so that the isolator was at the static equilibrium position. The electric vibration table was excited by harmonic excitations with the frequencies of 2, 3, 4, ..., 11 Hz and the amplitude of 5 mm. The laser vibration metre (Polytec PSV-400) was used to collect the response signals of the QZS prototype. The corresponding linear isolator without the two horizontal springs was also tested to collect its response signals under the same excitations. The displacement response of the electric vibration table was also acquired under the same frequencies by using the laser vibration meter. The root mean square (RMS) of

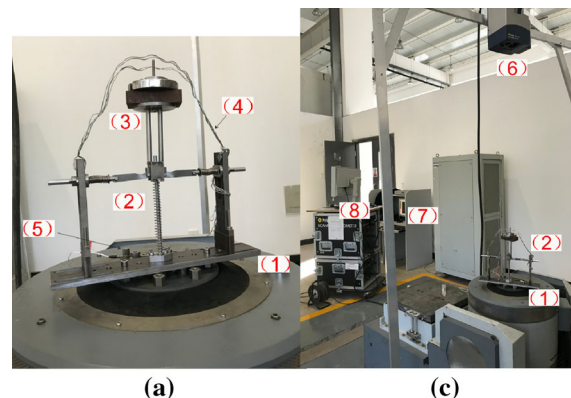


**Fig. 17** Dynamic tests and instruments (1) electric vibration table, (2) prototype of the QZS isolator composed of one pair of oblique bars (including the vertical spring leading to positive stiffness, one pair of oblique bars generating negative stiffness in the vertical direction, and the isolation platform), (3) the loaded mass, (4) iron wire for protecting isolator under large response amplitude, (5) accelerometer for electric vibration table, (6) Polytec PSV-400 scanning head, (7) the excitation signal controller of the electric vibration table, (8) vibrometer controller (Polytec PSV-400)

the amplitudes of the displacement responses was utilized to calculate the transmissibility.

The Polytec PSV-400 scanning head generates one laser point to the surface of the measured body. The laser point can be adjusted in a range of the measured surface by using the vibrometer controller. When the laser point is on the top surface of the electric vibration table, the vibrometer controller will record the output responses of the electric vibration table. When the laser point was on the top surface of the isolator, the vibrometer controller would record the responses of the isolator. Thus, the responses of the isolators and output responses of the electric vibration table could be measured by using the Polytec PSV-400 system.

The displacements of the electric vibration table measured by Polytec PSV-400 at 4 Hz, 6 Hz, 8 Hz and 10 Hz are shown in Fig. 18. The input signals for the electric vibration table are harmonic excitations with the amplitude of 5 mm. The amplitudes of the output signals of the electric vibration table measured by Polytec PSV-400 in Fig. 18 are calibrated to calculate displacement transmissibility.

The displacement responses of the QZS isolator and the corresponding linear isolator are, respectively,

acquired by using the laser vibrometer under the same displacement excitations as shown in Fig. 19, which shows that the improved QZS isolator has much better performance of vibration isolation than the corresponding linear isolator.

The absolute displacement transmissibility of the improved QZS isolator and that of the corresponding linear isolator measured by experiment are shown in Fig. 20. The values of the experimental transmissibility are calculated by the ratio of the RMS amplitudes between the measured displacement responses of isolators and the measured displacement output of the electric vibration table under different excitation frequencies. The theoretical displacement transmissibility can be calculated using Eq. in (26) [45]. The transmissibility of the improved QZS isolator is calculated using Eq. (26).

The displacement transmissibility of the improved QZS isolator has the initial frequency of vibration isolation lower than 4 Hz, and the initial frequency of vibration isolation of the corresponding linear isolator is about 7.5 Hz. The frequency band of vibration isolation of the QZS prototype is 3.5 Hz wider (towards low frequency) than the corresponding linear

**Fig. 18** Displacements of electric vibration table measured by Polytec laser vibrometer under the input excitation amplitude of 5 mm of the electric vibration table **a** 4 Hz, **b** 6 Hz, **c** 8 Hz, **d** 10 Hz

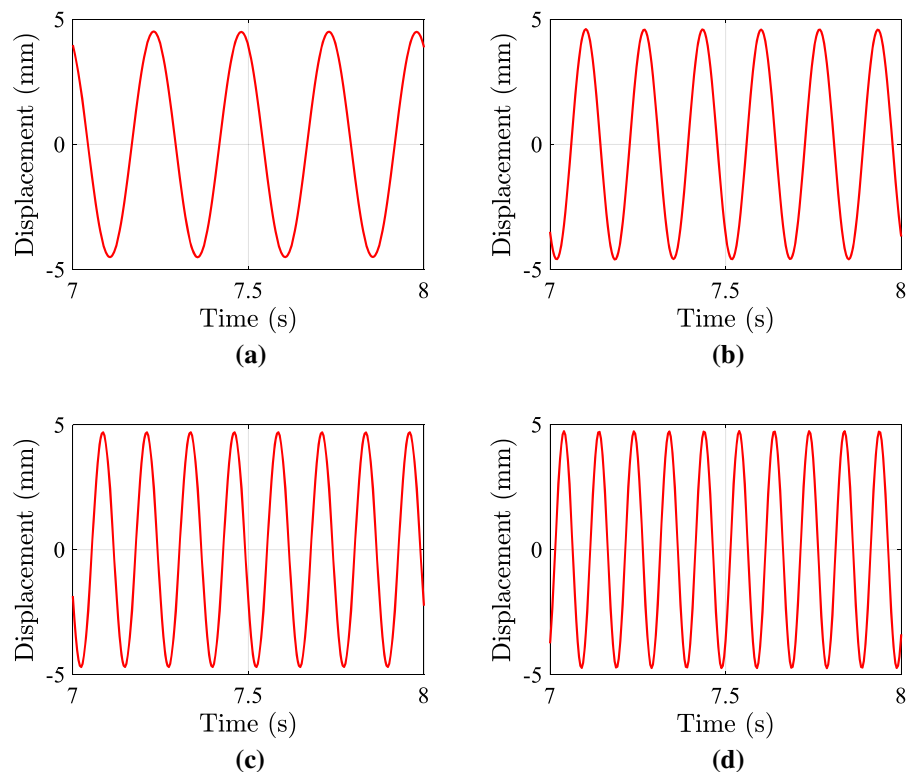


**Fig. 19** Displacement responses measured by Polytec laser vibrometer for the improved QZS isolator (red solid line) and the corresponding linear isolator (black dotted line), **a** 4 Hz, **b** 6 Hz, **c** 8 Hz, **d** 10 Hz

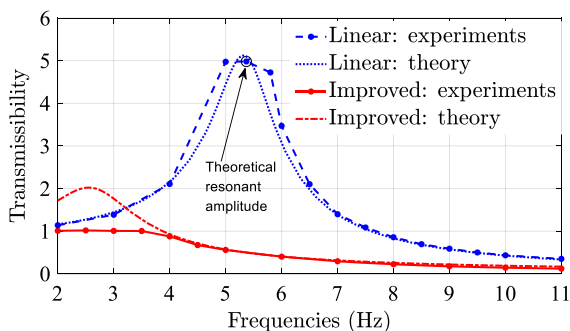
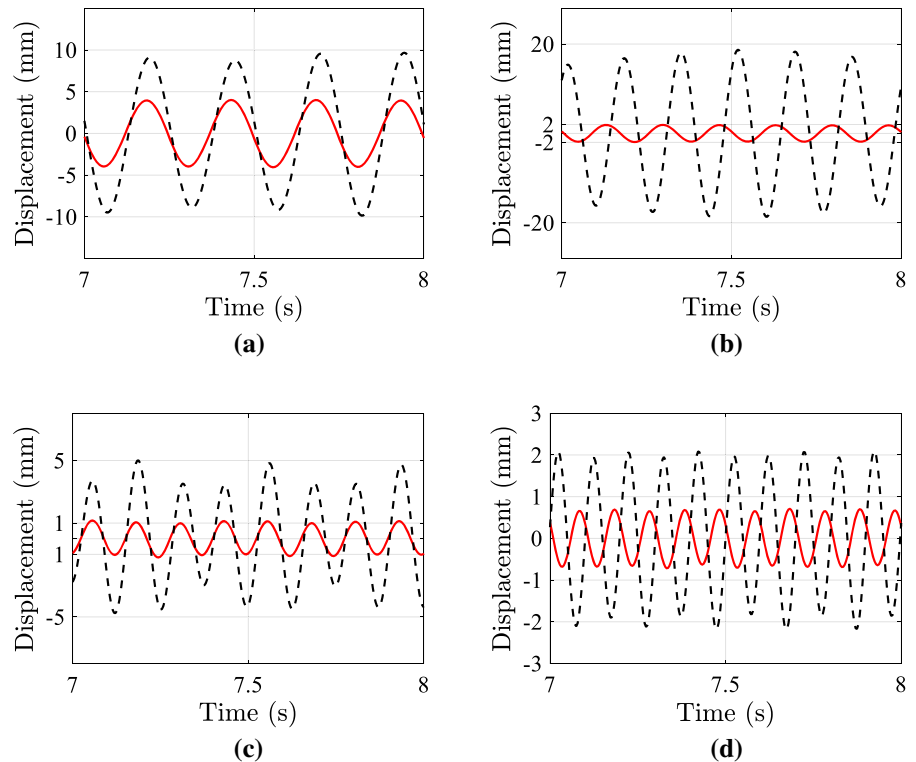


**Fig. 20** Absolute displacement transmissibility of the improved QZS isolator composed of one pair of oblique bars and the corresponding linear isolator under the same harmonic excitation amplitude of 5 mm

isolator. The transmissibility of the QZS prototype measured by experiment indicates that high damping effect in low frequency of resonance leads to small-amplitude response and small damping effect in high frequency generates small-amplitude response for the QZS isolator. In the resonant frequency range, a slight difference exists between the theoretical and experimental displacement transmissibility for the two isolators due to the damping effects. In the theoretical

transmissibility calculations, the damping ratio of the QZS isolator and the corresponding linear isolator is 0.15 and 0.1, respectively.

At the resonant frequency, the response of the corresponding linear isolator could not be obtained by experiment for safety reason due to the very large response amplitude. The peak amplitude at the resonant frequency of the corresponding linear isolator can be calculated by using:

$$B = \frac{\omega_0 Z_e}{2n} \quad (28)$$

where  $n = c/2m$  is the attenuation coefficient. The peak amplitude is shown in Fig. 20 at the resonant frequency of 5.37 Hz for the corresponding linear isolator.

## 6 Conclusions

A QZS isolator with one pair of oblique bars was further studied to develop a practical design principle. By considering the pre-compression of horizontal springs and setting the second-order derivative of



stiffness be zero, two conditions to obtain a constant QZS around the static equilibrium position were derived to provide some theoretical design guidelines for the QZS isolator with one pair of oblique bars. A prototype was designed and fabricated on the basis of the derived two equations to verify superior isolation performance of the improved QZS isolator.

In comparison with the existing QZS isolators with weak nonlinearity of stiffness, the improved design of QZS isolator could significantly increase the frequency band of vibration isolation and also isolate the large-amplitude vibrations, but also circumvent the transmissibility curve to bend right to mitigate external excitation with large amplitude. In comparison with the QZS isolator with one pair of oblique springs, the designed isolator with the constant QZS feature has a wider range of isolation frequency and lower transmissibility.

The experimental results showed that the absolute displacement transmissibility of the QZS prototype has a wider frequency band of vibration isolation than the corresponding linear isolator under the same mass load and vertical stiffness, especially small response around the resonant frequency range due to the friction between the linear bearing and guide rod. Theoretical analysis indicated that the zero second derivative of stiffness is an important condition to achieve constant QZS around the static equilibrium position and to widen frequency band in QZS isolators.

**Acknowledgements** This work is partially supported by National Natural Science Foundation of China (Grant No. 11872045).

**Funding** This work is supported by National Natural Science Foundation of China (Grant No. 11872045).

**Data availability** The authors confirm that data will be made available on reasonable request.

#### Declarations

**Conflict of Interest** The authors declare that they have no conflict of interest.

#### References

- Ji, J.C., Luo, Q.T., Ye, K.: Vibration control based meta-materials and origami structures: a state-of-the-art review. *Mech. Syst. Signal Process.* **161**, 107945 (2021)
- Ding, H., Ji, J.C., Chen, L.Q.: Nonlinear vibration isolation for fluid-conveying pipes using quasi-zero stiffness characteristics. *Mech. Syst. Signal Process.* **121**, 675–688 (2019)
- Sun, X.T., Wang, F., Xu, J.: Analysis, design and experiment of continuous isolation structure with Local Quasi-Zero-Stiffness property by magnetic interaction. *Int. J. Nonlinear. Mech.* **116**, 289–301 (2019)
- Ye, K., Ji, J.C.: An origami inspired quasi-zero stiffness vibration isolator using a novel truss-spring based stack miura-ori structure. *Mech. Syst. Signal Process.* **165**, 108383 (2022)
- Carrella, A., Brennan, M.J., Waters, T.P.: Static analysis of a passive vibration isolator with quasi-zero-stiffness characteristic. *J. Sound Vib.* **301**(3–5), 678–689 (2007)
- Kovacic, I., Brennan, M.J., Waters, T.P.: A study of a nonlinear vibration isolator with a quasi-zero stiffness characteristic. *J. Sound Vib.* **315**(3), 700–711 (2008)
- Zhao, F., Ji, J.C., Ye, K., Luo, Q.T.: Increase of quasi-zero stiffness region using two pairs of oblique springs. *Mech. Syst. Signal Process.* **144**, 106975 (2020)
- Zhao, F., Ji, J.C., Ye, K., Luo, Q.T.: An innovative quasi-zero stiffness isolator with three pairs of oblique springs. *Int. J. Mech. Sci.* **192**, 106093 (2021)
- Le, T.D., Ahn, K.K.: A vibration isolation system in low frequency excitation region using negative stiffness structure for vehicle seat. *J. Sound Vib.* **330**(26), 6311–6335 (2011)
- Le, T.D., Ahn, K.K.: Experimental investigation of a vibration isolation system using negative stiffness structure. *Int. J. Mech. Sci.* **70**, 99–112 (2013)
- Yang, T., Cao, Q.J., Li, Q.Q., Qiu, H.Q.: A multi-directional multi-stable device: modeling, experiment verification and applications. *Mech. Syst. Signal Process.* **146**, 106986 (2021)
- Liu, C.R., Yu, K.P.: A high-static-low-dynamic-stiffness vibration isolator with the auxiliary system. *Nonlinear Dyn.* **94**, 1549–1567 (2018)
- Bian, J., Jing, X.J.: Analysis and design of a novel and compact X-structured vibration isolation mount (X-Mount) with wider quasi-zero-stiffness range. *Nonlinear Dyn.* **101**, 2195–2222 (2020)
- Dong, Z., Shi, B.Y., Yang, J., Li, T.Y.: Suppression of vibration transmission in coupled systems with an inerter-based nonlinear joint. *Nonlinear Dyn.* **107**, 1637–1662 (2022)
- Li, M., Cheng, W., Xie, R.L.: A quasi-zero-stiffness vibration isolator using a cam mechanism with user-defined profile. *Int. J. Mech. Sci.* **189**, 105938 (2021)
- Ye, K., Ji, J.C., Brown, T.: A novel integrated quasi-zero stiffness vibration isolator for coupled translational and rotational vibrations. *Mech. Syst. Signal Process.* **149**, 107340 (2021)
- Ye, K., Ji, J.C., Brown, T.: Design of a quasi-zero stiffness isolation system for supporting different loads. *J. Sound Vib.* **471**, 115198 (2020)
- Zeng, R., Wen, G.L., Zhou, J.X., Zhao, G.: Limb-inspired bionic quasi-zero stiffness vibration isolator. *Acta. Mech. Sinica-PRC.* **37**(7), 1152–1167 (2021)
- Yan, G., Wang, S., Zou, H.X., Zhao, L.C., Gao, Q.H., Zhang, W.M.: Bio-inspired polygonal skeleton structure for

- vibration isolation: Design, modelling, and experiment. *Sci. China Technol. Sci.* **63**(12), 2617–2630 (2020)
20. Deng, T.C., Wen, G.L., Ding, H., Lu, Z.Q., Chen, L.Q.: A bio-inspired isolator based on characteristics of quasi-zero stiffness and bird multi-layer neck. *Mech. Syst. Signal Process* **145**, 106967 (2020)
  21. Yan, G., Zou, H.X., Wang, S., Zhao, L.C., Wu, Z.Y., Zhang, W.M.: Bio-inspired vibration isolation: methodology and design. *Appl. Mech. Rev.* **73**, 020801 (2021)
  22. Zhang, Q., Guo, D.K., Hu, G.K.: Tailored mechanical metamaterials with programmable quasi-zero-stiffness features for full-band vibration isolation. *Adv. Funct. Mater.* **31**, 2101428 (2021)
  23. Yan, B., Yu, N., Ma, H.Y., Wu, C.Y.: A theory for bistable vibration isolators. *Mech. Syst. Signal Process.* **167**, 108507 (2022)
  24. Liu, C.R., Yu, K.P., Liao, B.P., Hu, R.P.: Enhanced vibration isolation performance of quasi zero stiffness isolator by introducing tunable nonlinear inerter. *Commun. Nonlinear Sci.* **95**, 105654 (2021)
  25. Carrella, A., Brennan, M.J., Kovacic, I., Waters, T.P.: On the force transmissibility of a vibration isolator with quasi-zero-stiffness. *J. Sound Vib.* **322**(4–5), 707–717 (2009)
  26. Yang, T., Cao, Q.J., Hao, Z.F.: A novel nonlinear mechanical oscillator and its application in vibration isolation and energy harvesting. *Mech. Syst. Signal Process.* **155**, 107636 (2021)
  27. Wang, K., Zhou, J.X., Chang, Y.P., Ouyang, H.J., Xu, D.L., Yang, Y.: A nonlinear ultra-low-frequency vibration isolator with dual quasi-zero-stiffness mechanism. *Nonlinear Dyn.* **101**, 755–773 (2020)
  28. Zhao, F., Ji, J.C., Luo, Q.T., Cao, S.Q., Chen, L.M., Du, W.L.: An improved quasi-zero stiffness isolator with two pairs of oblique springs to increase isolation frequency band. *Nonlinear Dyn.* **104**, 349–365 (2021)
  29. Wang, X.J., Liu, H., Chen, Y.Q., Gao, P.: Beneficial stiffness design of a high-static-low-dynamic-stiffness vibration isolator based on static and dynamic analysis. *Int. J. Mech. Sci.* **142**, 235–244 (2018)
  30. Wang, Y., Li, H.X., Jiang, W.A., Ding, H., Chen, L.Q.: A base excited mixed-connected inerter-based quasi-zero stiffness vibration isolator with mistuned load. *Mech. Adv. Mater Struc.* online (2021)
  31. Zhang, L.X., Zhao, C.M., Qian, F., Dhupia, J.S., Wu, M.L.: A variable parameter ambient vibration control method based on quasi-zero stiffness in robotic drilling systems. *Machines* **9**(3), 67 (2021)
  32. Sun, X.T., Xu, J., Jing, X.J., Cheng, L.: Beneficial performance of a quasi-zero-stiffness vibration isolator with time-delayed active control. *Int. J. Mech. Sci.* **82**, 32–40 (2014)
  33. Zhao, L., Yu, Y., Zhou, C., Yang, F.: Modelling and validation of a seat suspension with rubber spring for off-road vehicles. *J. Vib. Control* **24**(18), 4110–4121 (2018)
  34. Le, T.D., Nguyen, V.A.D.: Low frequency vibration isolator with adjustable configurative parameter. *Int. J. Mech. Sci.* **134**, 224–233 (2017)
  35. Dai, W., Yang, J.: Vibration transmission and energy flow of impact oscillators with nonlinear motion constraints created by diamond-shaped linkage mechanism. *Int. J. Mech. Sci.* **194**, 106212 (2021)
  36. Cheng, C., Li, S., Wang, Y., Jiang, X.: Force and displacement transmissibility of a quasi-zero stiffness vibration isolator with geometric nonlinear damping. *Nonlinear Dyn.* **87**, 2267–2279 (2017)
  37. Zhang, X.H., Cao, Q.J., Huang, W.H.: Dynamic characteristics analysis for a quasi-zero-stiffness system coupled with mechanical disturbance. *Arch. Appl. Mech.* **91**(4), 1449–1467 (2021)
  38. Jing, X.J., Zhang, L.L., Jiang, G.Q., Feng, X., Guo, Y.Q., Xu, Z.D.: Critical factors in designing a class of X-shaped structures for vibration isolation. *Eng. Struct.* **199**, 109659 (2019)
  39. Song, Y., Zhang, C., Li, Z.L., Li, Y., Lian, J.Y., Shi, Q.L., Yan, B.J.: Study on dynamic characteristics of bio-inspired vibration isolation platform. *J. Vib. Control.* online (2021)
  40. Sun, X.T., Wang, F., Xu, J.: A novel dynamic stabilization and vibration isolation structure inspired by the role of avian neck. *Int. J. Mech. Sci.* **193**, 106166 (2021)
  41. Li, M., Cheng, W., Xie, R.: Design and experiments of a quasi-zero-stiffness isolator with a noncircular cam-based negative-stiffness mechanism. *J. Vib. Control.* **26**(21–22), 1935–1947 (2020)
  42. Li, M., Cheng, W., Xie, R.: Design and experimental validation of a cam-based constant-force compression mechanism with friction considered. *P. I Mech. Eng. C-J Mech.* **233**(11), 3873–3887 (2019)
  43. Papaioannou, G., Voutsinas, A., Koulocheris, D.: Optimal design of passenger vehicle seat with the use of negative stiffness elements. *P. I Mech Eng. D-J Aut.* **234**(2–3), 610–629 (2020)
  44. Yang, J., Xiong, Y.P., Xing, J.T.: Dynamics and power flow behaviour of a nonlinear vibration isolation system with a negative stiffness mechanism. *J. Sound Vib.* **332**(1), 167–183 (2013)
  45. Carrella, A., Brennan, M.J., Waters, T.P., Lopes, V., Jr.: Force and displacement transmissibility of a nonlinear isolator with high-static-low-dynamic-stiffness. *Int. J. Mech. Sci.* **55**(1), 22–29 (2012)

**Publisher's Note** Springer Nature remains neutral with regard to jurisdictional claims in published maps and institutional affiliations.